Supporting Information for

Effects of Post-Transfer Annealing and Substrate Interactions on the Photoluminescence of 2D/3D Monolayer WS_2/Ge Heterostructures

Tianyi Zhang[1,2#], Andrew Voshell[3#], Da Zhou[2,4#], Zachary D. Ward[5], Zhuohang Yu[1,2], Mingzu Liu[2,4], Kevin O. Díaz Aponte[3], Tomotaroh Granzier-Nakajima[2,4], Yu Lei[2,4,6], He Liu[2,7], Humberto Terrones[5], Ana Laura Elías[8], Mukti Rana[3], Mauricio Terrones[1,2,4,7*]*

[*]Corresponding author: Mauricio Terrones, mut11@psu.edu; Mukti Rana, mrana@desu.edu

[#]These authors contributed equally to the work

[1]Department of Materials Science and Engineering, The Pennsylvania State University, University Park, PA 16802, USA

[2]Center for 2-Dimensional and Layered Materials, The Pennsylvania State University, University Park, PA 16802, USA

[3]Division of Physics, Engineering, Mathematics and Computer Sciences and Optical Science Center for Applied Research, Delaware State University, Dover, DE 19901, USA

[4]Department of Physics, The Pennsylvania State University, University Park, PA 16802, USA

[5]Department of Physics, Applied Physics and Astronomy, Rensselaer Polytechnic Institute, Troy, NY 12180, USA

[6]Institute of Materials Research, Tsinghua Shenzhen International Graduate School, Tsinghua University, Shenzhen 518055, China

[7]Department of Chemistry, The Pennsylvania State University, University Park, PA 16802, USA

[8]Department of Physics, Binghamton University, Binghamton, NY 13902, USA

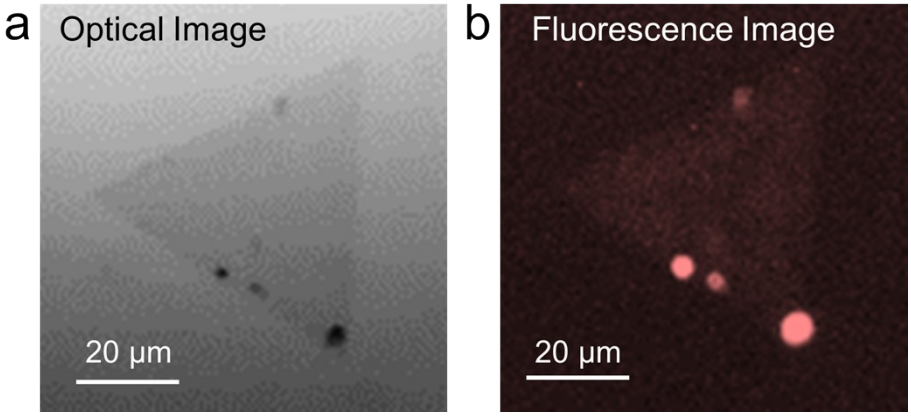

Figure S1. Typical (a) optical and (b) fluorescence images of monolayer WS_2/Ge heterostructures. A weak fluorescence emission intensity is observed in WS_2/Ge heterostructures.

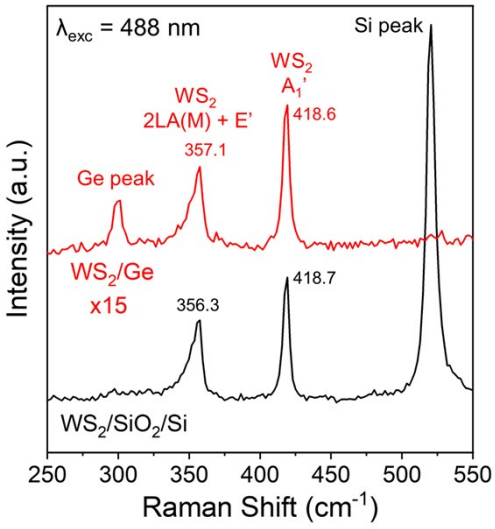

Figure S2. Raman spectra of as-grown WS_2 on SiO_2/Si and WS_2/Ge (annealed) obtained with a 488 nm laser. Note that WS_2/Ge heterostructures display a much weaker Raman signal, and the corresponding Raman spectrum data (red) is multiplied by 15 for visualization.

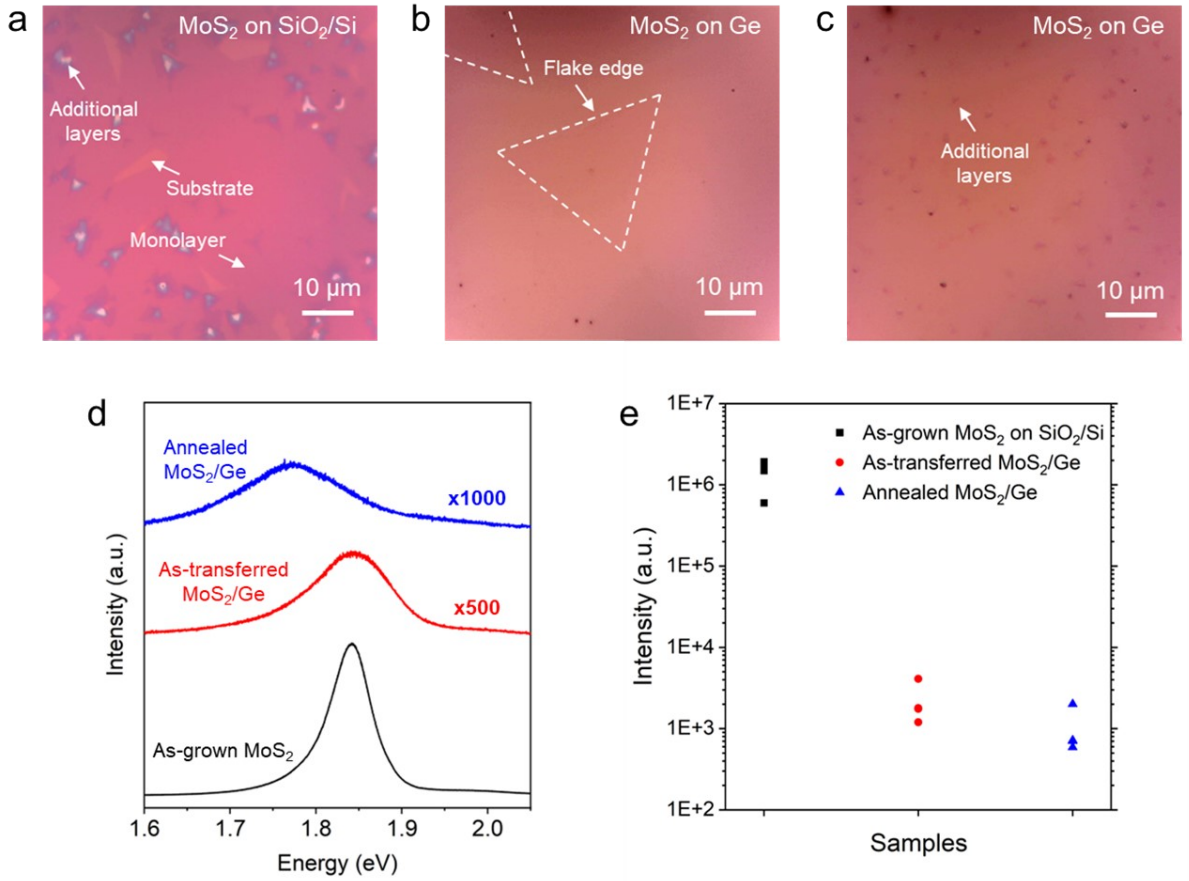

Figure S3. PL studies of MoS_2/Ge heterostructures and effects of post-transfer annealing, in which the monolayer MoS_2 is grown on SiO_2/Si by CVD and then transferred to Ge. (a) Optical image of as-grown monolayer MoS_2 on SiO_2/Si. The monolayer MoS_2, bare substrate, and additional MoS_2 layer regions are distinguished by optical contrast and marked by white arrows. **(b)** Optical image of typical MoS_2 flakes transferred on Ge. **(c)** Optical image of continuous films of monolayer MoS_2 on Ge. MoS_2 monolayers exhibit low optical contrast on Ge. **(d)** A comparison of PL spectra of as-grown monolayer MoS_2, as-transferred MoS_2/Ge, and annealed MoS_2/Ge. MoS_2/Ge heterostructures display prominent PL intensity quenching compared to as-grown MoS_2. **(e)** A plot of PL intensity distributions of the samples investigated in (d). For each case, four random spots are measured, so that the spatial variation of PL intensity is taken into account.

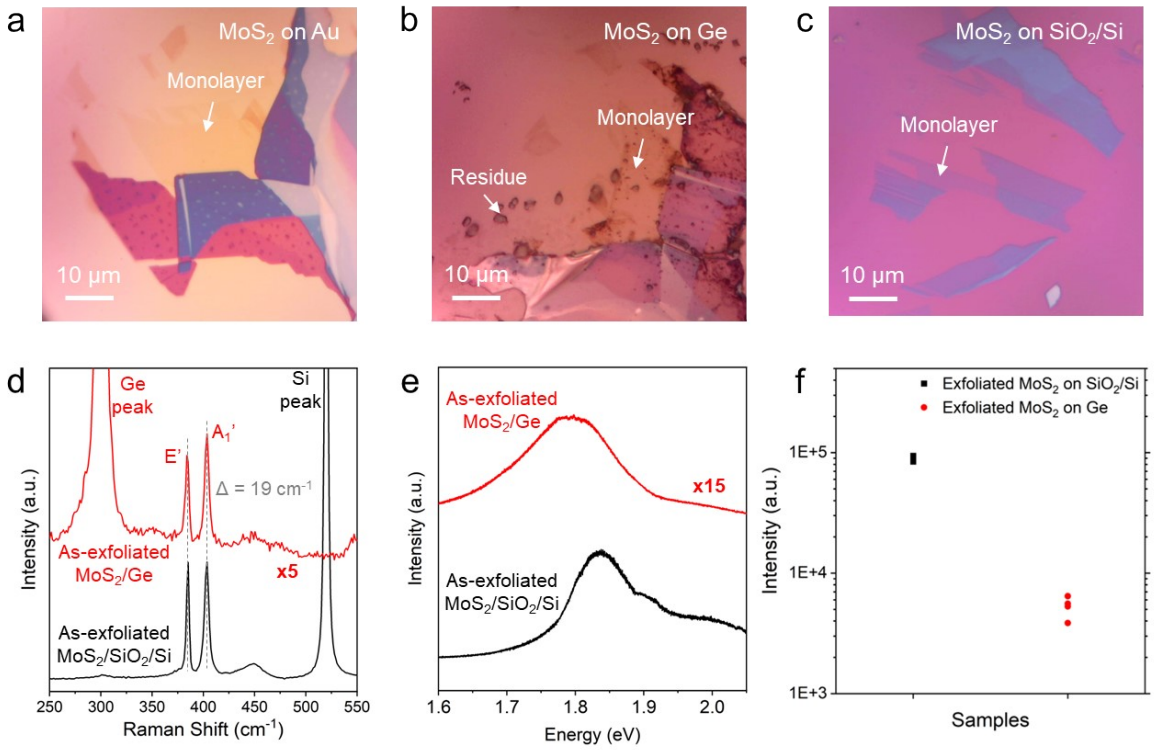

Figure S4. PL studies of MoS_2/Ge heterostructures obtained by exfoliating monolayer MoS_2 on Ge. Considering the very low optical contrast of TMD monolayers on Ge, a previously reported gold (Au)-assisted approach was adopted to increase the exfoliation yield and aid the identification of monolayers.[1] **(a)** Optical image of a MoS_2 flake exfoliated on a gold tape (consisting of Au(150 nm)/PMMA/thermal release tape (TRT)), in which the monolayer region can be distinguished based on optical contrast. **(b)** Optical image of the identical flake transferred onto Ge. The monolayer MoS_2 region can be determined by comparing this optical image with (a). **(c)** Optical image of a monolayer MoS_2 exfoliated on SiO_2/Si. **(d)** Raman spectra of exfoliated MoS_2/SiO_2/Si and MoS_2/Ge. The monolayer nature of these flakes can be verified by the separation (~19 cm^{-1}) between E' and A_1' Raman modes.[2, 3] **(e)** A comparison of PL spectra of exfoliated MoS_2/SiO_2/Si and MoS_2/Ge. It should be noted that we were not able to obtain the PL spectra of annealed MoS_2/Ge, as our current exfoliation approach resulted in surface residue on both the MoS_2 flakes and Ge substrate. The residue seemed to be aggregated on top of the MoS_2 flake during the annealing process, hindering further optical characterizations. Future work is required to improve

our exfoliation technique in order to study the exfoliated MoS_2/Ge heterostructures in detail. **(f)** A plot of PL intensity distributions of the samples investigated in (e). For each case, four random spots are measured, so that the spatial variation of PL intensity is taken into account.

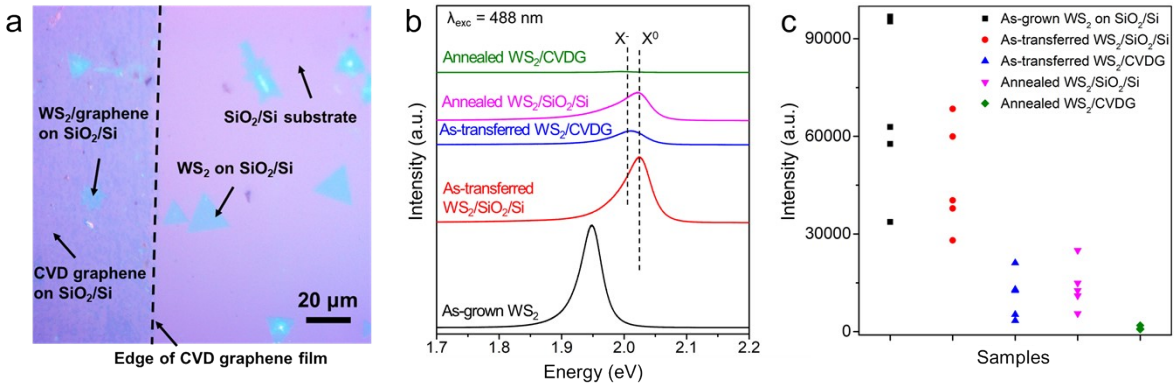

Figure S5. Effects of post-transfer annealing on the PL intensity and uniformity of $WS_2/SiO_2/Si$ and WS_2/CVD-grown monolayer graphene (CVDG)/SiO_2/Si heterostructures. **(a)** Optical image of monolayer WS_2 transferred on CVDG/SiO_2/Si. The left side of the SiO_2/Si substrate is covered with CVDG (purple colored region) while the right side of the substrate is without CVDG. Thus, both $WS_2/SiO_2/Si$ and WS_2/CVDG/SiO_2/Si can be found and measured within this sample. **(b)** A comparison of PL spectra of as-grown monolayer WS_2, as-transferred $WS_2/SiO_2/Si$, annealed $WS_2/SiO_2/Si$, as-transferred WS_2/CVDG/SiO_2/Si, and annealed WS_2/CVDG/SiO_2/Si. **(c)** A plot of PL intensity distributions of the samples investigated in (b). For each case, five random spots are measured, so that the spatial variation of PL intensity is taken into account. The results indicate a consistent PL intensity quenching and uniformity improvement after the low-pressure Ar/H_2 annealing process.

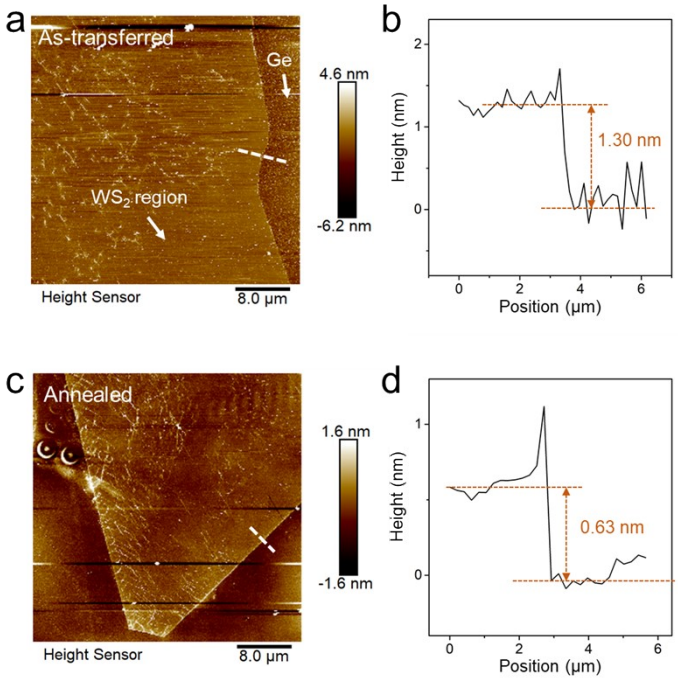

Figure S6. Additional AFM data of as-transferred and annealed WS_2/Ge heterostructures, which were obtained from different flakes with the data presented in Figures 2e-h. (a) AFM topography image of as-transferred WS_2/Ge and **(b)** the corresponding surface height profile along the white dashed line in (a). **(c)** AFM topography image of annealed WS_2/Ge and **(d)** the corresponding surface height profile along the white dashed line in (c). The reduction of WS_2/Ge distance is consistently observed.

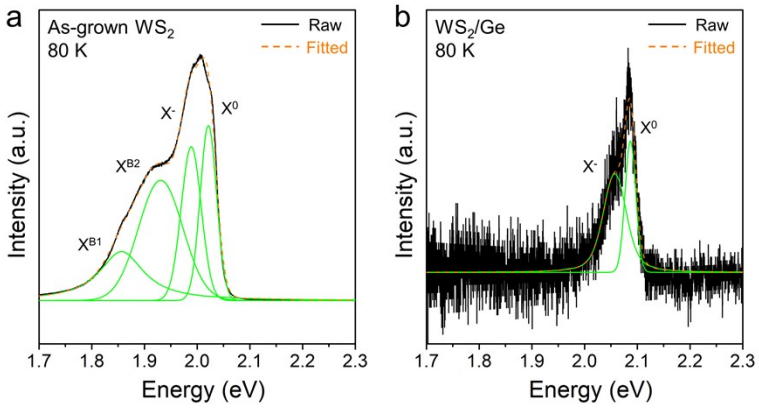

Figure S7. PL spectra of as-grown WS_2 and WS_2/Ge heterostructures measured at 80 K. The spectra were deconvoluted and exciton species were determined by peak fitting using Voigt

profiles. Individual peaks are plotted with green solid lines, while the cumulative fitted spectra are plotted with orange dashed lines.

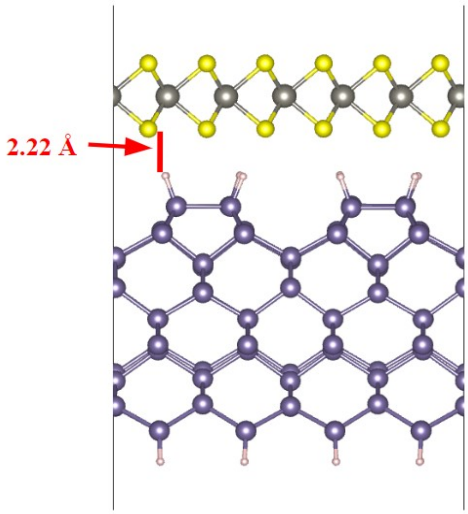

Figure S8. DFT-calculated structure of WS_2/H-Ge(100). The distance between the topmost H atoms and topmost S atoms is calculated to be 2.22 Å.

References

1. F. Liu, W. Wu, Y. Bai, S. H. Chae, Q. Li, J. Wang, J. Hone and X. Y. Zhu, *Science*, 2020, **367**, 903-906.
2. C. Lee, H. Yan, L. E. Brus, T. F. Heinz, J. Hone and S. Ryu, *ACS Nano*, 2010, **4**, 2695-2700.
3. M. Buscema, G. A. Steele, H. S. J. van der Zant and A. Castellanos-Gomez, *Nano Research*, 2014, **7**, 561-571.